ISTITUTO NAZIONALE FISICA NUCLEARE

INFN/AE - 78/8
14 Dicembre 1978

N. Grion and B. Saitta:

DESCRIPTION OF A PLASTIC SCINTILLATOR TELESCOPE USED AS A PION BEAM MONITOR IN EXPERIMENTS OF NEGATIVE PION CAPTURE AT REST IN NUCLEI

SERVIZIO RIPRODUZIONE DELLA
SEZIONE DI TRIESTE DELL'INFN

DESCRIPTION OF A PLASTIC SCINTILLATOR TELESCOPE USED AS A PION BEAM MONITOR IN EXPERIMENTS OF NEGATIVE PION CAPTURE AT REST IN NUCLEI

N. Grion and B. Saitta
Istituto Nazionale Fisica Nucleare - Sezione di Trieste
Italy

ABSTRACT

A fast plastic scintillator telescope has been set up in order to monitor a pion beam in connection with experiments of negative pion capture at rest in nuclei where the kinematical quantities of the emitted particles are measured using the time of flight technique. The beam telescope was able to furnish, by means of its good timing properties and fast-particle-discrimination capabilities, the number and the intrinsic time dispersion of the pion stopped in the target without muon and electron contamination. A pure electron fast gate signal, very useful to calibrate neutron and charged particle detectors, was also available.

By studying the effects of the energy degrader material on both the time distribution and the intensity of the particles of the incoming beam we have verified that a low energy and a good momentum definition are two necessary characteristics of a pion beam for carrying out experiments in which negative pions are absorbed at rest in "thin" targets.

1. - INTRODUCTION

In experiments where negative pions are captured at rest in nuclei and the kinematical characteristics of the emitted particles (neutrons, protons, deuterons, etc.) are measured employing the time of flight (TOF) technique, the main requirements for the incoming pion beam are:

1) pions of low energy ($\lesssim$30 MeV). This is necessary for two reasons:
   a) to minimize the thickness of the degrader material that the pions must go through before their stop in the target;
   b) to be far from the maximum of the pion-nucleus total cross section of the slowing down material;
2) good pion momentum definition and high intensity, in order to maximize the number of stopped pions;
3) low muon and electron contamination, to reduce the general background in the experiment.

While requirement 2) is well satisfied by the modern meson factories, both requirements 1) and 2) are simultaneously available only at the Triumf meson facility. In any case the presence of muons and electrons in the pion beam is unavoidable because these particles are produced by the decay in flight of the pions themselves. Generally, the percentage of the electrons present in the beams extracted from cyclotrons, is comparable with that of the pions (*). The electron contamination is a source of troubles in experiments in which the negative pions are absorbed at rest because they easily simulate pions stopped in the target and because they contribute to the background of the experimental area.

On the other hand the knowledge of the absolute number of the pions stopped in the target and their time (or energy) distribution is an essential information in these experiments in order to be able to normalize the spectra of the emitted particles, to obtain the branching ratios of the reactions involved and to calculate the true jitter of the start signal.

(*) see for instance "Triumf Annual Report 1975", "SIN Newsletter N°8(1977)" and the results reported in this report.

In order to reduce as much as possible the electron contamination and to know the number and the time distribution of the stopped pions we have set up a beam telescope having the characteristics and the performances described in this report.

2. - BEAM TELESCOPE

The beam telescope is shown in Fig. 1. The distances between the detectors, their number and dimensions have been chosen in such a manner to satisfy simultaneously the following conditions:

a) to stop the maximun number of particles in the target;
b) to detect only stopped pions;
c) to have the minimun pion time dispersion between CT2 and the target.

The TOF measurements of the beam particles (*) is performed by the CT1 (NE104, 20x10x1 cm^3) and CT2 (NE104, 20x20x1 cm^3) detectors. Their relative distance must be chosen in such a way to obtain a clear separation between the three components; it depends on the timing resolution of experimental apparatus and on the energies of the incoming beam particles. In particular CT2 must be placed before the degrader in order to test the time composition of the incoming beam anytime it is necessary.

In Fig. 2(a) the TOF spectrum of the incoming beam particles (**) without aluminium absorber is shown.

The following information can be derived:
- relative percentage of three components $N_\pi : N_\mu : N_e$ = 65%:23%:12%;
- pion energy at the CT2 position 67.7 MeV;
- energy and momentum dispersion 5% and 3% respectively.

The aluminium degrader is placed after CT2. Its presence causes a serie of negative effects on the beam intensity and structure which can be

---

(*) The measurements was carryed out at the LEPC channel of the CERN 600 MeV Synchro-cyclotron (SC).

(**) The incoming beam particles is the beam monitored by the coincidence CT1xCT2x$\overline{CA1}$x$\overline{CM2}$x$\overline{CA2}$.

evaluated from the following data.

1) The structure and the intensity of the beam impinging upon the target (*) when the aluminium thickness (6.1 cm) corresponds to the maximum of the pion stopping rate in the target is shown in Fig. 2(b). As for Fig. 2(a), the data that can be deduced are:

   - relative percentage of the three components $N_\pi : N_\mu : N_e$ = 44%:41%:15%;
   - pion energy at the CT2 position 68.3 MeV;
   - energy and momentum dispersion 5% and 3% respectively.

   From a comparison of the two results it is clear that there is a drastic reduction of the number of pions incident upon the target after the aluminium insertion. In our case the loss is of 78%; of this loss a fraction of 13% is due to the decay in flight, while a fraction of 65% is due to the scattering of pions by the absorber nuclei (moreover 1% must be attributed to the air thickness present between CT2 and the target and to the thickness of the CM2).

   A further small reduction due to the pion fast discrimination (**) must be considered: it decreases the intensity of the pion beam component of 2%. When this is added to the reduction due to the aluminium absorber, the total loss of the number of pions impinging upon the target amounts to 80%.

(*) In these measurements a liquid helium target was employed. The helium, at atmospheric pressure and at 4 K temperature, was filling a cylindrical cell having 2 cm of thickness and 20 cm of diameter. The total thickness of the mylar windows surrounding the target was 1.2 mm thick. The helium gas consumption of the target in stable work condition was only of 280 l/h.

(**) This operation, which is described in the next paragraph, allow to select optionally anyone of the three beam components.

2) The kinetic energy distribution that the pions stopped in the target exhibit at CT2 and just before entering in the target are shown in Fig. 3 and 4 respectively (*). The large loss in energy definition of the pions stopped in the target, after the insertion of the aluminium degrader, increases the intrinsic pion time dispersion which from 170 psec (FWHM) becomes 560 psec (FWHM) at the target position. When the TOF technique is used to determine the energies of the particles produced by the pion absorption in the target, the relative error associated to the energies the detected particles is given by the formula:

$$\frac{\Delta\tau}{\tau} \simeq 2 \frac{\Delta t}{t} \cdot f(\beta^2)$$

where t is the TOF of the particle, $f(\beta^2)$ a function of β^2 and Δt the start-stop time indetermination. In our case, the large value of the intrinsic pion time dispersion at their target arrival, increases the total start time indetermination up to 610 psec in spite of the fact that the electronic start time indetermination of our beam telescope is 250 psec (**).

Another negative consequence of the large energy dispersion of the pions emerging from the aluminium degrader is a further 50% reduction of the number of pions stopped in the target, so that we are able to stop only 10% of the pions present in the incoming beam.

(*) These energy distributions have been deduced from the TOF spectra and taking into account the energy losses suffered by the pions in air, in the scintillator material and in the aluminium degrader.

(**) The electronic start-stop time indetermination of our beam telescope for electrons is FWHM = 350 psec. If we assume that it is the same for the start and stop, the electronic start time indetermination can be evaluated to be 250 psec.

In order to limit as much as possible the losses discussed above and to get rid of the muons, produced by the pion decays in flight, simulating pions stopped in the target, the set of detectors CT2, CA1, CM2 and CA2 must be as much close to each other as possible. In particular, either the distance between CM2 and CA2 (*) and the thickness of CM2 must be minimized.

The detectors CA1 (NE110, 20x30x0.5 cm^3, Ø10 cm) and CM2 (NE110, 10x10x0.05 cm^3) are geometrically placed in such a way that CM2 works as a coincidence counter while CA1 works as an anticoincidence counter. This combination selects particles of the beam of well defined trajectories, so that one can neglect their flight path differences between CT2 and the target.

On the other hand the electrons of the beam scattered from the aluminium and striking the light pipes of CM2 are detected through Čerenkov radiation. These electrons also escape CA2 and then simulate a particle stopped in the target. By means of CA1 it is possible partially to reject these electrons by choosing suitable dimensions for CA1. In the Fig. 5(a) and 5(b) the time distribution of the particles stopped in the target (**) are shown. We can see the electron peak near the pion peak. The exact knowledge of this particular electron contamination is necessary to normalize the measurements to the true number of stopped pions, since it is 6% and 31% in two cases respectively, and therefore not negligible.

The CA2 detector (NE110, 41x21x0.5 cm^3, Ø7 cm) selects the beam on the target and the anticoincidence CA3 (NE104, 30x20x0.5 cm^3) rejects the particles that are not stopped in the target.

(*) CM2 can be put near to CA2 up to the point that the charged particles produced in the target and going out through the hole of CA2 are not intercepted.

(**) The incoming beam used to obtain the Fig. 5(a) is shown in Fig. 2(a), while that one relative to Fig. 5(b) is a beam having $N_\pi : N_\mu : N_e$ = 46%: :6%:48% and τ_π = 101.0 MeV.

3. - ELECTRONIC ARRANGEMENT

In Fig. 6 the block diagram of the electronics is shown. The timing circuit, already described in ref. 1, for both CT1 and CT2, consists of two 473 constant fraction timing discriminators, two shaper cable timed and one mean-timer. It is used to get the beam particles time distribution.

The fast discrimination between the three beam components is performed by means of a logic circuit: by using a long distance between CT1 and CM2 (521 cm) and high resolution discriminators (FWHM of the output signal = 2 nsec) we have obtained the coincidence curve shown in Fig 7. Such curve does not resolves the three beam components, but it is clear that choosing different values of the delay used in the coincidence curve within the range 24-41 nsec, one can discriminate different components of the incoming beam. In the same figure the evaluated contribution of the three components of the beam entering in the target are rapresented by the dotted lines.

By enabling the ORTEC 457 time-to-amplitude converter with the CT1xCT2x$\overline{\text{CM2}}$x$\overline{\text{CA2}}$ (*) output signal we have obtained the results shown in Fig. 8 in which the three components of the beam are well discriminated from each other. Then, with an easy changement of a delay value, we can realize a fast gate signal depending either from the electron component or the pion component (with a small muon contamination) of the beam. As it is reported by several authors, the electron fast gate signal is very useful to calibrat the neutron and charged particle detectors (left-right pulse height equaliz electron equivalent threshold setting, etc.) and to compensate their output signal time differences (ref. 2).

By gating the ORTEC 457 time-to-amplitude converter with the CT1xCT2x $\overline{\text{CM2}}$x$\overline{\text{CA2}}$x$\overline{\text{CA3}}$ output signal, we have obtained the time distribution of the pions stopped in the target (see Fig. 5(a) and 5(b)). When the pion fast discrimination is introduced, electronically the muon and electron contamins are almost completely eliminated as it is shown in Fig. 5(c).

(*) The symbol —— means "not", and $\overline{\text{CM2}}$ = $\overline{\text{CA1xCM2}}$.

REFERENCES

(1) C. Cernigoi, N. Grion and G. Pauli, Nucl. Instr. and Meth. 131 (1975) 495.

(2) F.P. Brady, J.A. Jungerman, J.C. Young, J.L. Romero and P.S. Symonds, Nucl. Instr. and Meth. 58 (1968) 57-60.
G. Gatti, P. Hillman, W.C. Middelkoop, T. Yamagata and E. Zavattini, Nucl. Instr. and Meth. 29 (1964) 77-82.

P.A. Bernardo, R.P. Haddock, L. Verhey and M.E. Zeller, Nucl. Instr. and Meth. 79 (1970) 43-50.

FIGURE CAPTIONS

Fig. 1 - Simplified view of the beam telescope.

Fig. 2 - TOF spectrum and time calibration of the incoming beam particles:
a) without aluminium absorber;
b) with the aluminium absorber thickness (6.1 cm) corresponding to the maximum of the negative pion stopping rate in the target.

Fig. 3 - Kinetic energy distribution, at the position of the CT2 counter, of the pion stopped in the target.

$\Delta\tau$ (FWHM)/τ(EVERAGE VALUE) = 3%.

Fig. 4 - Kinetic energy distribution, at the position of the CA2 counter of the pion stopped in the target. $\Delta\tau/\tau$ = 50%

Fig. 5 - TOF spectrum of the pions stopped in the target with the aluminium thickness corresponding to the maximum of the negative pion stopping rate in the target. The ORTEC 457 was enabled by the $CT1xCT2x\overline{CM2}x\overline{CA2}x\overline{CA3}$ output signal:
a) pion fast discrimination not used. The incoming beam particles is that shown in Fig. 2.
b) pion fast discrimination not used. The incoming beam particles had the following characteristics:
$N_\pi:N_\mu:N_e$ = 46%:6%:48%, τ_π = 101.0 MeV.
c) as a) but with the pion fast discrimination in operation.

Fig. 6 - Block diagram of the electronics. The symbol D means delay.

Fig. 7 - CT1xCM2 coincidence curve. The experimental points are fitted by hand.

Fig. 8 - TOF spectrum of the incoming beam particles with 6.1 cm of aluminium thickness. The ORTEC 457 was enabled by the $CT1xCT2x\overline{CM2}x\overline{CA2}$ output signal and the particles fast discrimination was used:
a) pion fast discrimination. It corresponds to a delay value of 29 nsec in the $CT1x\overline{CM2}$ coincidence curve. The percentage of the three beam components are $N_\pi:N_\mu:N_e$ = 91%:9%:0%;

b) muon fast discrimination. The delay value is 33 nsec and the percentage are $N_\pi : N_\mu : N_e$ = 12%:78%:10%;

c) electron fast discrimination. The delay value is 39 nsec and the percentage are $N_\pi : N_\mu : N_e$ = 0%:1%:99%.

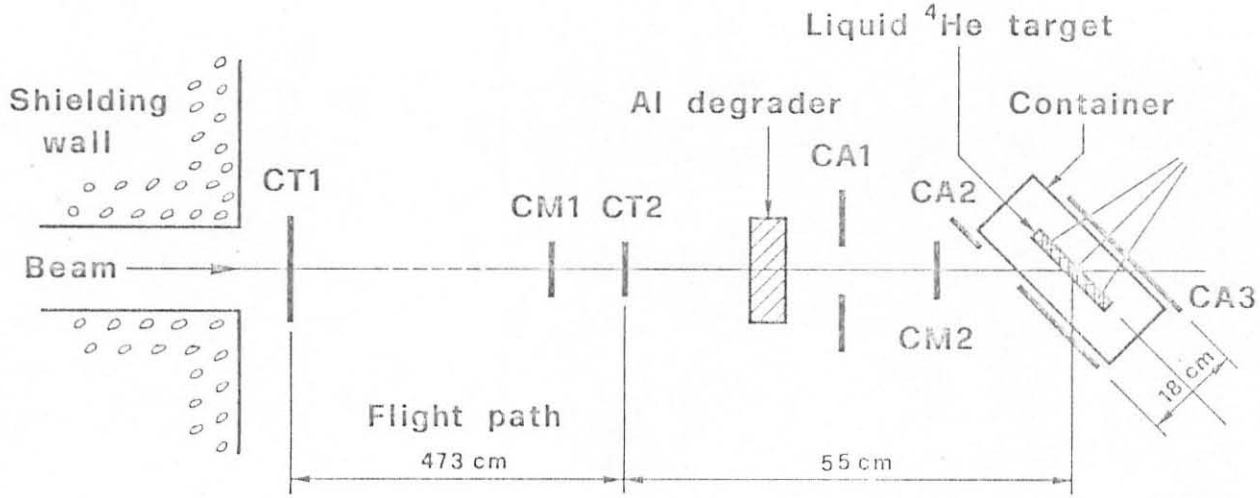
Liquid ^{4}He target
Shielding wall
Al degrader
Container
CA1
CT1
CM1
CT2
CA2
Beam
CA3
CM2
18 cm
Flight path
473 cm
55 cm

FIG.1

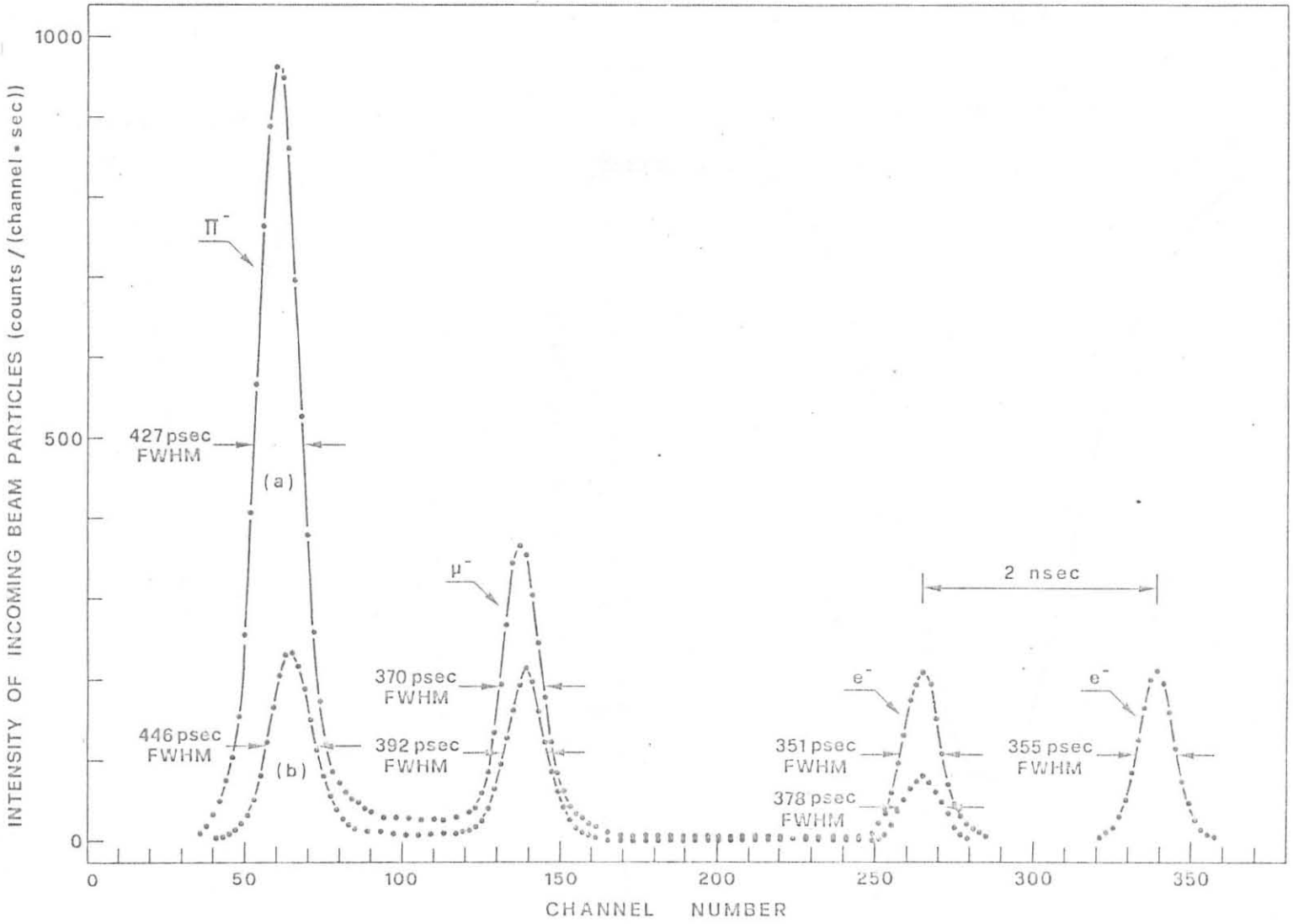
INTENSITY OF INCOMING BEAM PARTICLES (counts / (channel • sec))
1000
500
0
0
50
100
150
200
250
300
350
CHANNEL NUMBER
π⁻
427 psec FWHM
(a)
446 psec FWHM
(b)
μ⁻
370 psec FWHM
392 psec FWHM
2 nsec
e⁻
351 psec FWHM
378 psec FWHM
e⁻
355 psec FWHM

FIG. 2

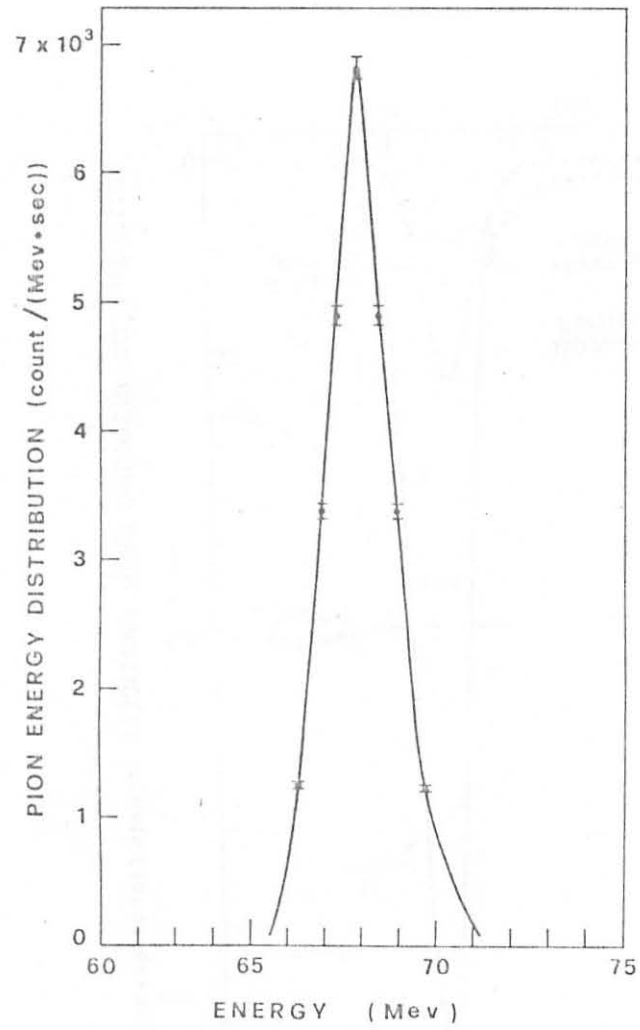
7 x 10³
6
5
4
3
2
1
0
PION ENERGY DISTRIBUTION (count/(Mev•sec))
60
65
70
75
ENERGY (Mev)

FIG. 3

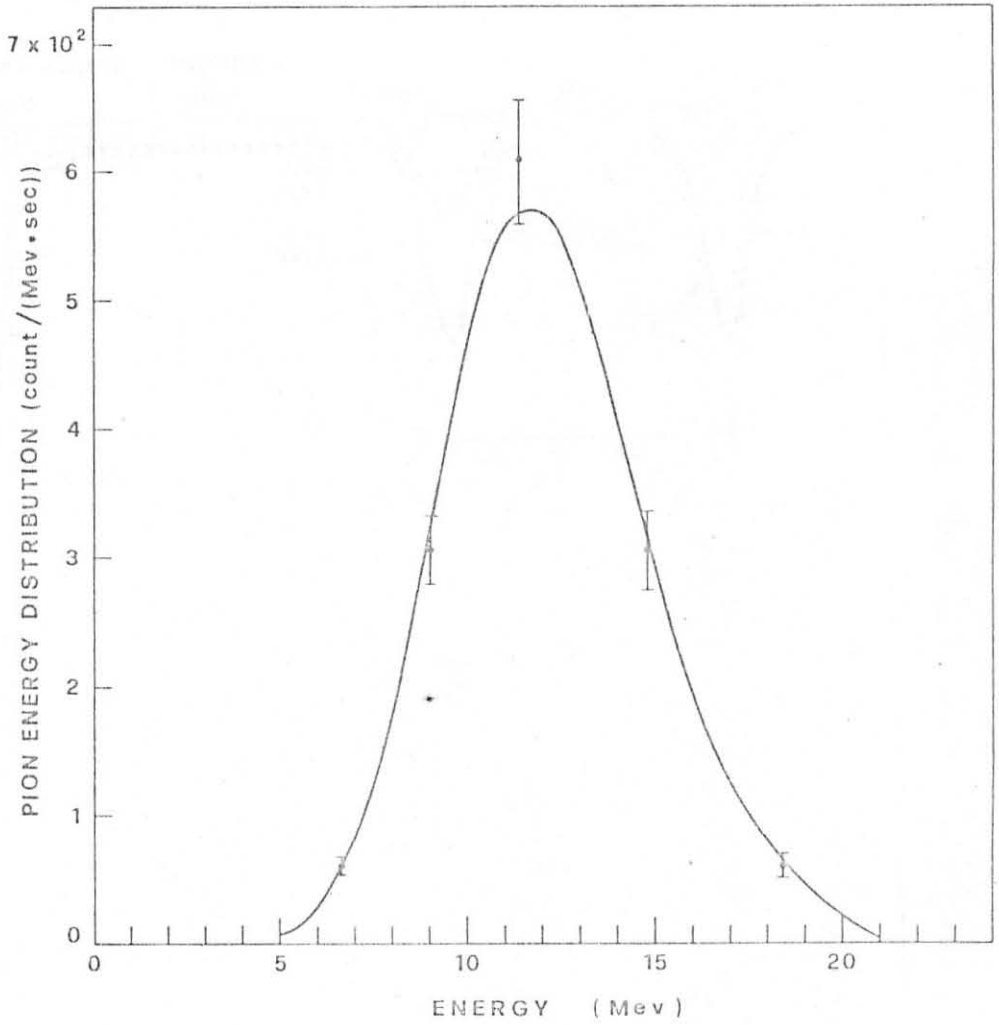
7 x 10²
6
5
4
3
2
1
0
PION ENERGY DISTRIBUTION (count/(Mev•sec))
0
5
10
15
20
ENERGY (Mev)

FIG. 4

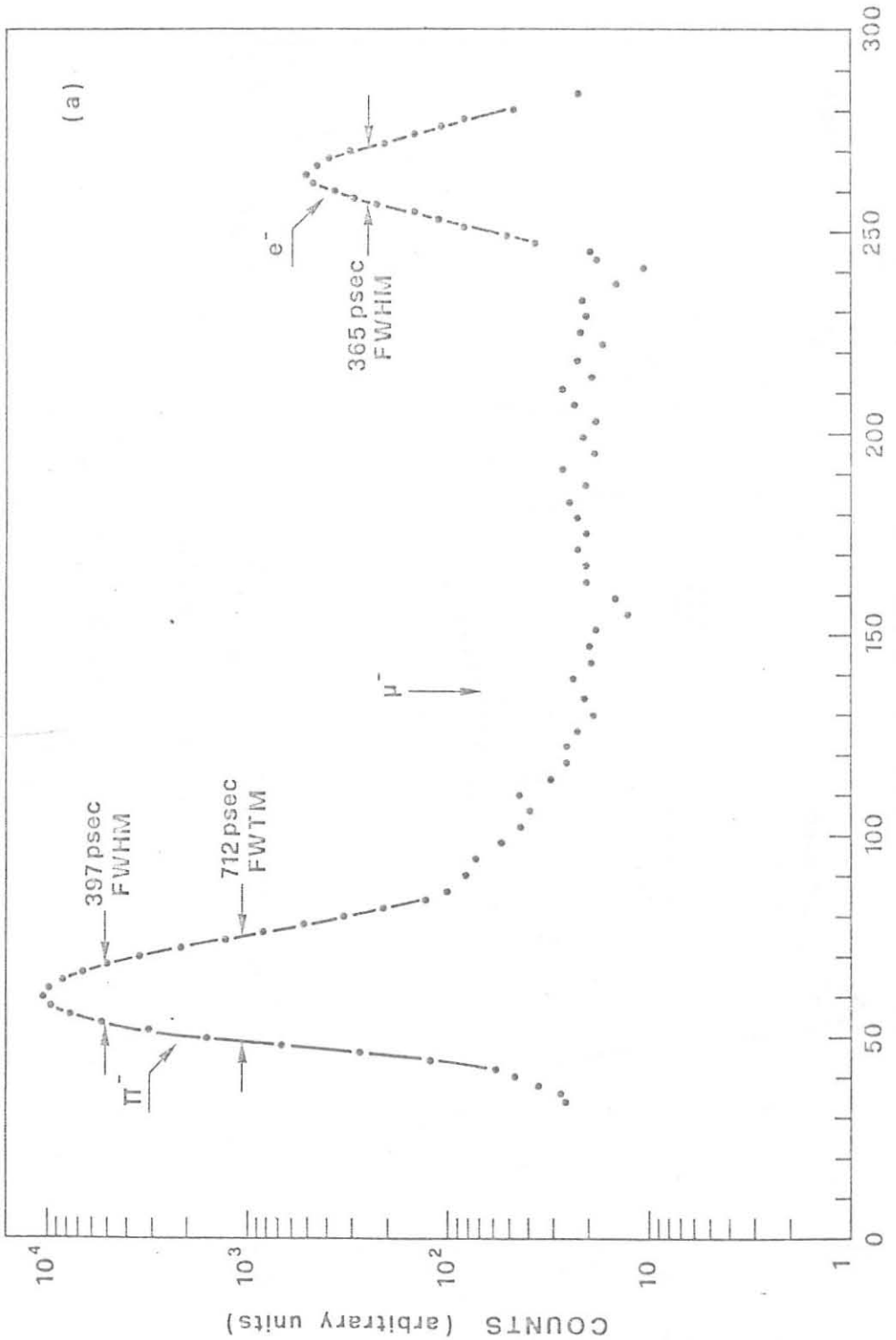
(a)
397 psec FWHM
712 psec FWTM
365 psec FWHM
π⁻
μ⁻
e⁻
COUNTS (arbitrary units)
CHANNEL NUMBER
10⁴
10³
10²
10
1
0
50
100
150
200
250
300

FIG. 5

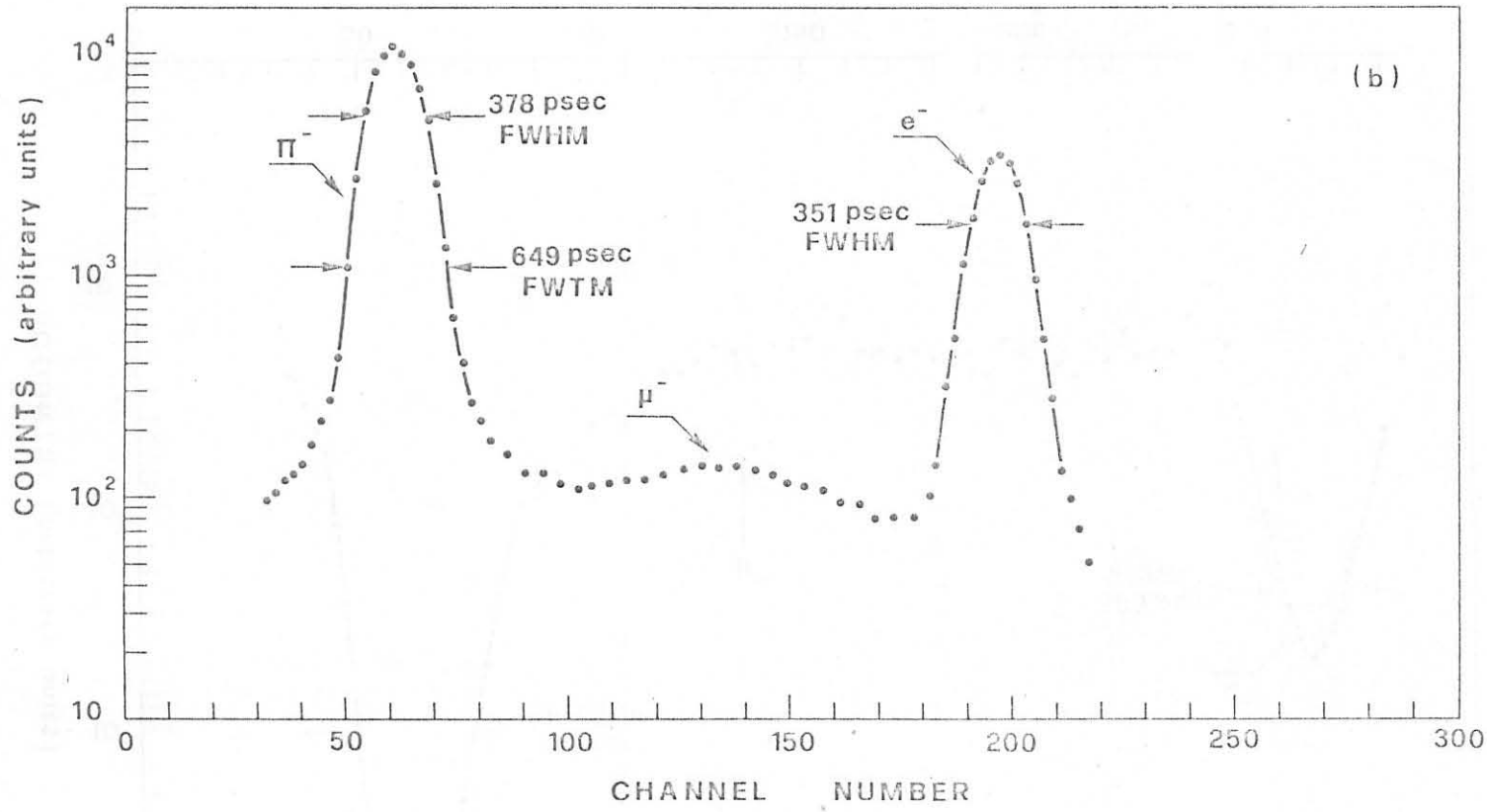
(b)
COUNTS (arbitrary units)
10^4
10^3
10^2
10
π^-
378 psec
FWHM
649 psec
FWTM
μ^-
e^-
351 psec
FWHM
0
50
100
150
200
250
300
CHANNEL NUMBER

FIG. 5

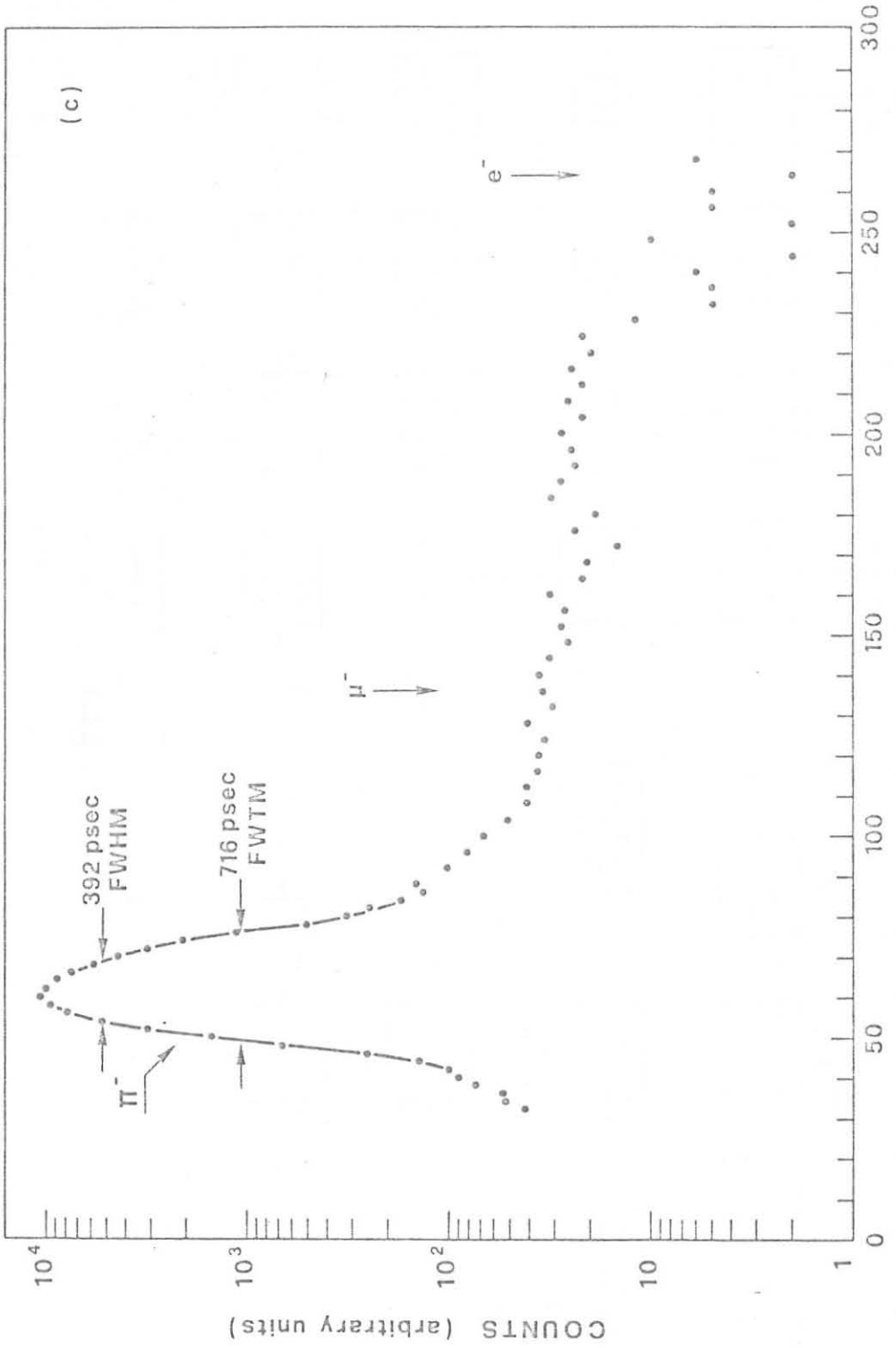
(c)
392 psec FWHM
716 psec FWTM
π⁻
μ⁻
e⁻
COUNTS (arbitrary units)
CHANNEL NUMBER
10⁴
10³
10²
10
1
0
50
100
150
200
250
300

FIG. 5

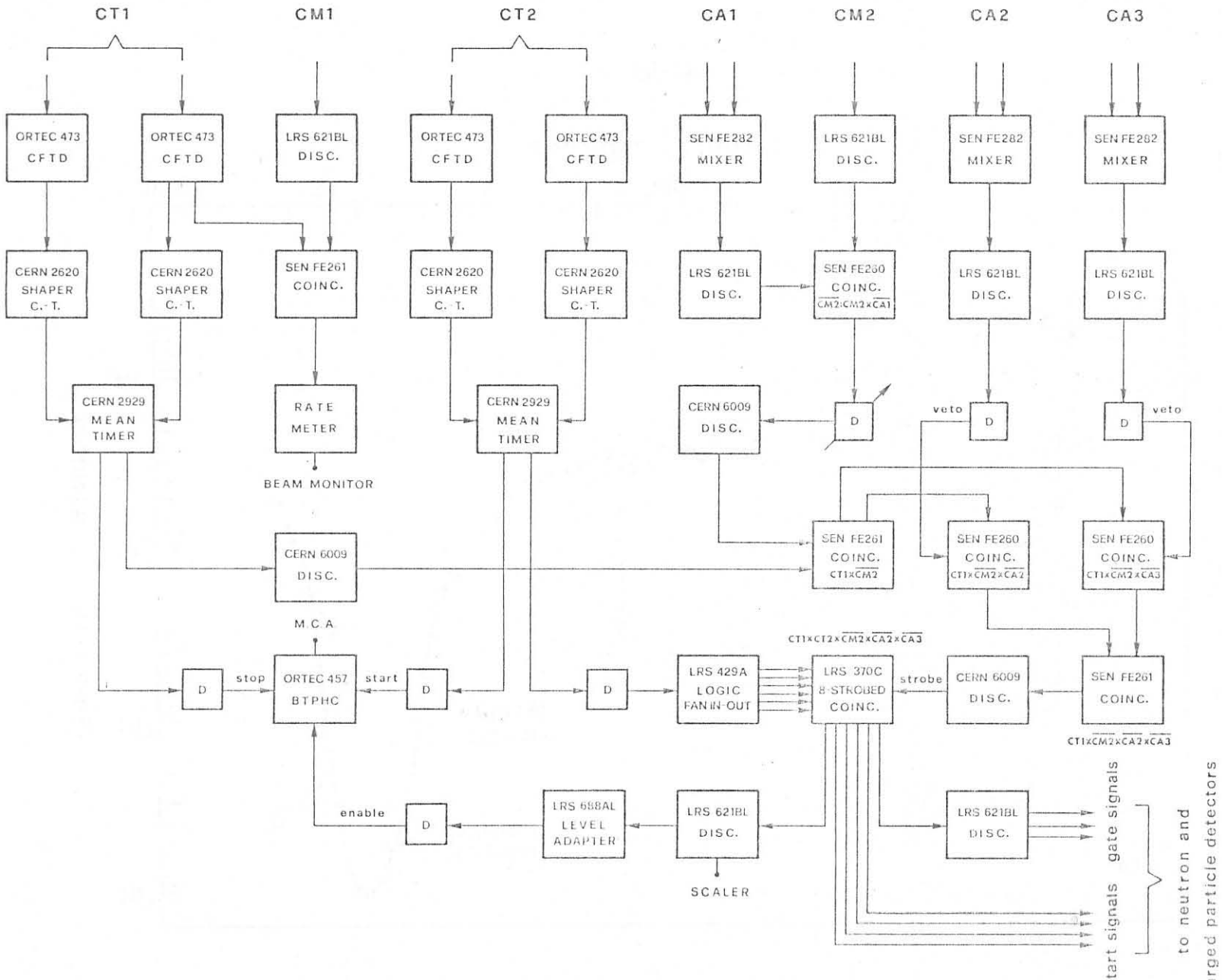
CT1
CM1
CT2
CA1
CM2
CA2
CA3
ORTEC 473 CFTD
ORTEC 473 CFTD
LRS 621BL DISC.
ORTEC 473 CFTD
ORTEC 473 CFTD
SEN FE282 MIXER
LRS 621BL DISC.
SEN FE282 MIXER
SEN FE282 MIXER
CERN 2620 SHAPER C.-T.
CERN 2620 SHAPER C.-T.
SEN FE261 COINC.
CERN 2620 SHAPER C.-T.
CERN 2620 SHAPER C.-T.
LRS 621BL DISC.
SEN FE260 COINC. CM2·CM2×CA1
LRS 621BL DISC.
LRS 621BL DISC.
CERN 2929 MEAN TIMER
RATE METER
BEAM MONITOR
CERN 2929 MEAN TIMER
CERN 6009 DISC.
D
veto
D
D
veto
CERN 6009 DISC.
SEN FE261 COINC. CT1×CM2
SEN FE260 COINC. CT1×CM2×CA2
SEN FE260 COINC. CT1×CM2×CA3
M.C.A
CT1×CT2×CM2×CA2×CA3
D
stop
ORTEC 457 BTPHC
start
D
D
LRS 429A LOGIC FAN-IN-OUT
LRS 370C 8-STROBED COINC.
strobe
CERN 6009 DISC.
SEN FE261 COINC.
CT1×CM2×CA2×CA3
enable
D
LRS 688AL LEVEL ADAPTER
LRS 621BL DISC.
LRS 621BL DISC.
SCALER
start signals
gate signals
to neutron and
charged particle detectors

FIG.6

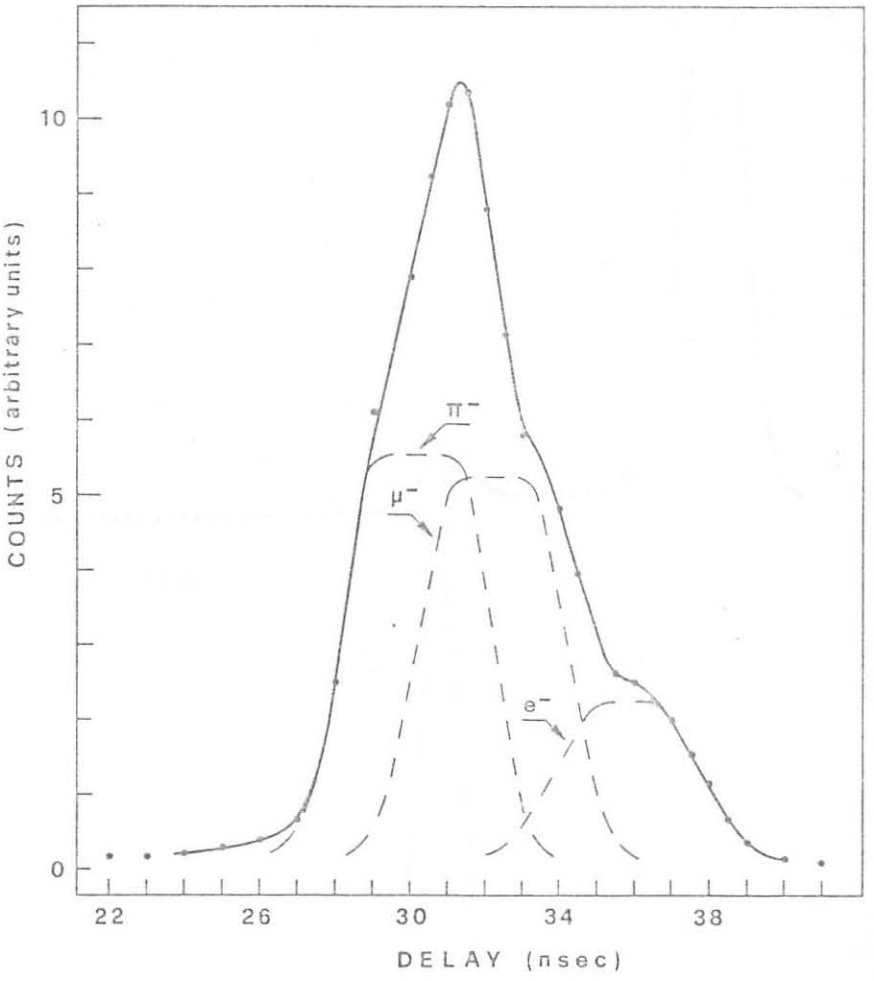

FIG.7

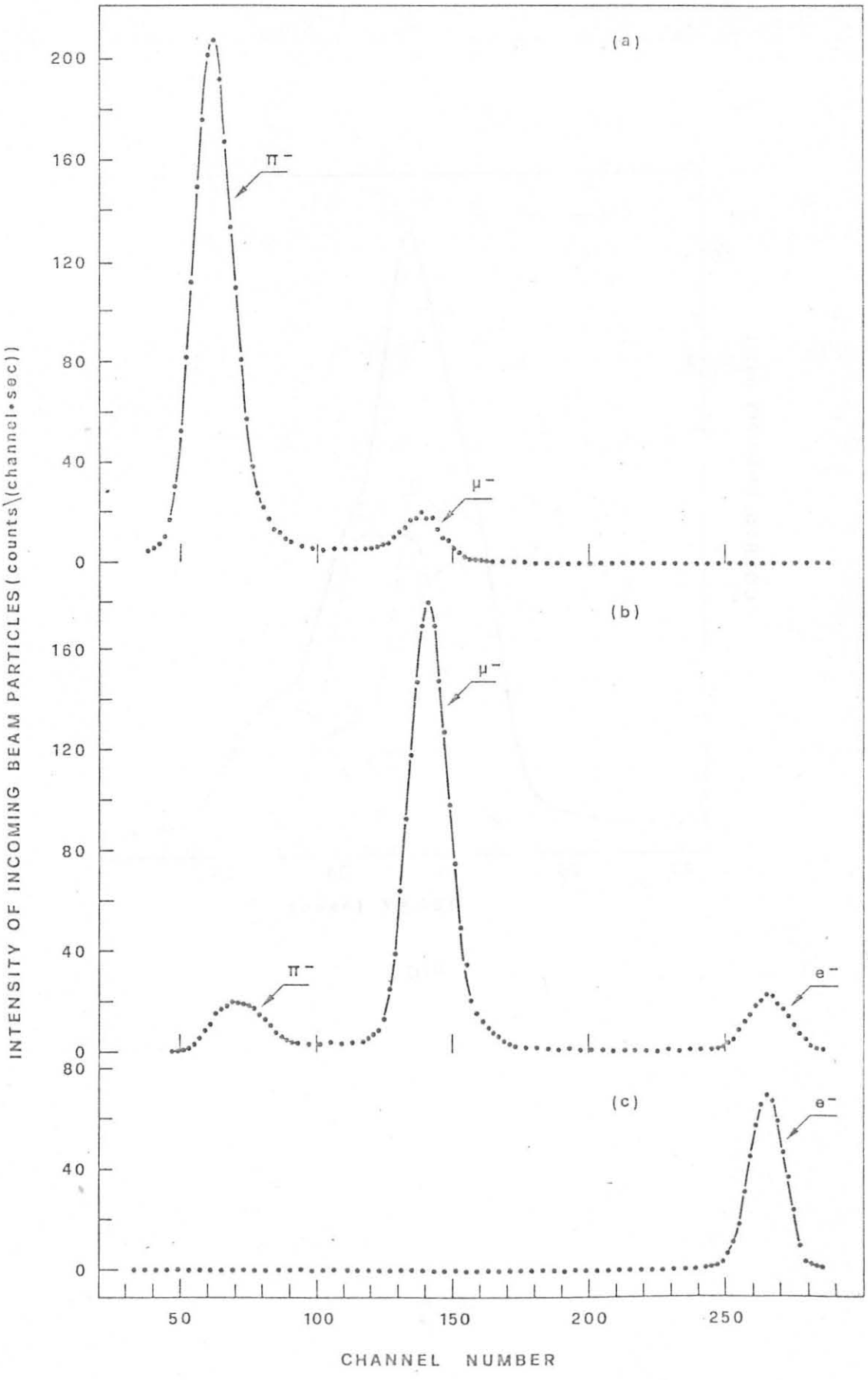
(a)
π⁻
μ⁻
(b)
μ⁻
π⁻
e⁻
(c)
e⁻
200
160
120
80
40
0
160
120
80
40
0
80
40
0
50
100
150
200
250
INTENSITY OF INCOMING BEAM PARTICLES (counts\(channel•sec))
CHANNEL NUMBER

FIG.8